An Improved Weighted Essentially Non-Oscillatory Scheme for Hyperbolic Conservation Laws

Rafael Borges [*] Bruno Costa [†] Wai Sun Don [‡]

June 23, 2006

Abstract

We develop in this article an improved version of the fifth-order weighted essentially non-oscillatory (WENO) scheme. Through the novel use of higher order information already present in the framework of the classical scheme, new smoothness indicators are devised and we obtain a new WENO scheme with less dissipation than the classical WENO of Jiang and Shu [2], with the same computational cost, and a slightly better performance than the improved mapped version of Henrick et al [3]. We show that the enhancements of the new scheme come from its ability to assign substantially larger weights to discontinuous stencils than the previous versions of WENO. Numerical experiments with the linear advection of discontinuous functions and the one dimensional Euler system of equations are conducted to demonstrate the benefit of using this improved version of the WENO scheme for hyperbolic conservation laws.

Keywords
Weighted Essentially Non-Oscillatory, Hyperbolic Conservation Laws

AMS
65P30, 77Axx

1 Introduction

In the numerical simulation of compressible flows modeled by means of hyperbolic conservation laws in the form

$$\frac{\partial u}{\partial t} + \boldsymbol{\nabla} \cdot F(u) = 0, \tag{1}$$

the development of finite time discontinuities generates $O(1)$ oscillations, known as the Gibbs phenomenon, causing loss of accuracy and numerical instability. Among many choices of shock capturing numerical schemes such as the Piecewise Parabolic method (PPM) [7], the Essentially Non-Oscillatory scheme (ENO) [6], high order Weighted Essentially Non-Oscillatory schemes (WENO) [1, 2] have been extensively used for the simulation of the fine scale and delicate structures of the physical phenomena related to shock-turbulence interactions.

WENO schemes owe their success to the use of a dynamic set of stencils, where a nonlinear convex combination of lower order polynomials adapts either to a higher order approximation at smooth parts

[*]Departamento de Matemática Aplicada, IM-UFRJ, Caixa Postal 68530, Rio de Janeiro, RJ, C.E.P. 21945-970, Brazil. E-Mail: rborges@ufrj.br

[†]Departamento de Matemática Aplicada, IM-UFRJ, Caixa Postal 68530, Rio de Janeiro, RJ, C.E.P. 21945-970, Brazil. E-Mail: bcosta@ufrj.br

[‡]Division of Applied Mathematics, Brown University, Providence, Rhode Island 02912. E-Mail: wsdon@cfm.brown.edu

Report Documentation Page

Form Approved
OMB No. 0704-0188

1. REPORT DATE	2. REPORT TYPE	3. DATES COVERED
23 JUN 2006		**00-06-2006 to 00-06-2006**

4. TITLE AND SUBTITLE	5a. CONTRACT NUMBER
An Improved Weighted Essentially Non-Oscillatory Scheme for Hyperbolic Conservation Laws	5b. GRANT NUMBER
	5c. PROGRAM ELEMENT NUMBER
6. AUTHOR(S)	5d. PROJECT NUMBER
	5e. TASK NUMBER
	5f. WORK UNIT NUMBER
7. PERFORMING ORGANIZATION NAME(S) AND ADDRESS(ES) **Brown University,Division of Applied Mathematics,182 George Street,Providence,RI,02912**	8. PERFORMING ORGANIZATION REPORT NUMBER
9. SPONSORING/MONITORING AGENCY NAME(S) AND ADDRESS(ES)	10. SPONSOR/MONITOR'S ACRONYM(S)
	11. SPONSOR/MONITOR'S REPORT NUMBER(S)

12. DISTRIBUTION/AVAILABILITY STATEMENT
Approved for public release; distribution unlimited

13. SUPPLEMENTARY NOTES
The original document contains color images.

14. ABSTRACT

15. SUBJECT TERMS

16. SECURITY CLASSIFICATION OF:			17. LIMITATION OF ABSTRACT	18. NUMBER OF PAGES	19a. NAME OF RESPONSIBLE PERSON
a. REPORT **unclassified**	b. ABSTRACT **unclassified**	c. THIS PAGE **unclassified**		**15**	

of the solution, or to an upwind spatial discretization that avoids interpolation across discontinuities and provides the necessary dissipation for shock capturing. The nonlinear coefficients of the convex combination, hereafter referred to as weights, are based on the local smoothness indicators, which measure the sum of the normalized squares of the scaled L^2 norms of all derivatives of the lower order polynomials [2]. An essentially zero weight is assigned to those lower order polynomials whose underlining stencils contain high gradients and/or shocks, yielding an essentially non-oscillatory solution at discontinuities. At smooth regions, higher order is achieved through the mimicking of the central upwinding scheme of maximum order, when all smoothness indicators are about the same size. Hence, an efficient design of these smoothness indicators is a very important issue for WENO schemes.

The classical choice of smoothness indicators in [2] generated weights that failed to recover the maximum order of the scheme at critical points of the solution. This fact was clearly pointed out at Henrick et al. [3]. In their study, necessary and sufficient conditions on the weights, for optimality of the order, were derived and a correcting mapping to be applied to the classical weights was devised. The resulting mapped WENO scheme of [3] recovered the optimal order of convergence at critical points and presented sharper results close to discontinuities. In this article, we follow a different approach, which is to improve on the classical smoothness indicators to obtain weights that satisfies the sufficient conditions for optimal order. Taylor series analysis of the classical smoothness indicators reveals that a simple combination of them would give higher order information about the regularity of the numerical solution. The incorporation of this new higher order information into the weights definition improves the convergence order at smooth parts of the solution, as well as decreases dissipation close to discontinuities, while maintaining stability and an essentially non-oscillatory behavior.

The enhancements of the new scheme come from the bigger weights that it assigns to discontinuous stencils. Contrary to common belief, the strategy should be to augment the influence of the stencil containing the discontinuity as much as possible, without destroying the essentially non-oscillatory behavior. A comparison of the weights of the classical, the mapped and the new WENO scheme close to a discontinuity shows that the ratio between the weight of a discontinuous stencil and a continuous one increases slightly from the classical weights to the mapped weights, and increases substantially with the new weights proposed in this article. This was made possible through the use of higher order smoothness indicators already available at the definition of the classical weights.

This paper is organized as follows: In Section 2, the classical WENO scheme of Jiang and Shu [2] and the mapped weights version of Henrick et al. [3] are described and some of the relevant analytical results are reviewed. The new WENO scheme is introduced at Section 3 where a detailed discussion about the new smoothness indicators is given. In Section 4, we perform a numerical comparison of all the schemes in the linear advection of discontinuous functions and in the solution of the one dimensional Euler equations in the classical cases of the shock density wave interaction and the interactive blastwaves problems.

2 Weighted essentially non-oscillatory schemes

In this section we describe the fifth order weighted essentially non-oscillatory conservative finite difference scheme when applied to hyperbolic conservation laws as in (1). Without loss of generality, we will restrict our discussion in this article to the one dimensional scalar case. Extensions to system of equations and higher spatial dimensions present no extra complexity with regards to our main point which is the design of new smoothness indicators for the WENO scheme.

Consider an uniform grid defined by the points $x_i = i\Delta x, i = 0, \ldots, N$, which are also called cell centers, with cell boundaries given by $x_{i+\frac{1}{2}} = x_i + \frac{\Delta x}{2}$. The semi-discretized form of (1) by the method of lines, yields a system of ordinary differential equations

$$\frac{du_i(t)}{dt} = -\left.\frac{\partial f}{\partial x}\right|_{x=x_i}, \quad i = 0, \ldots, N, \tag{2}$$

where $u_i(t)$ is a numerical approximation to the point value $u(x_i, t)$.

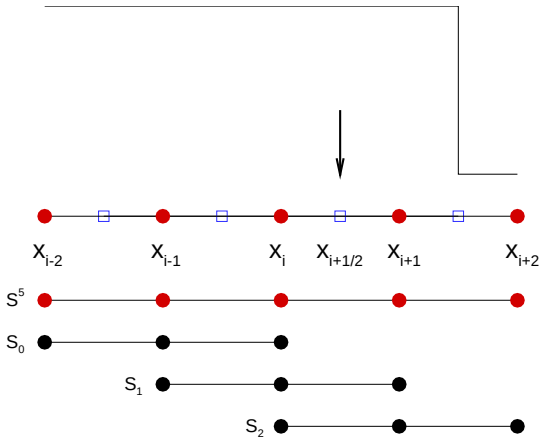

Figure 1: The computational uniform grid x_i and the total 5-points stencil S^5, composed of the three 3-points stencils $S_k, k = 0, 1, 2$, used for the fifth order WENO reconstruction.

A conservative finite-difference formulation for hyperbolic conservation laws requires high-order consistent numerical fluxes at the cell boundaries in order to form the flux difference across the uniformly-spaced cells. The conservative property of the spatial discretization is obtained by implicitly defining the numerical flux function $h(x)$ as

$$f(x) = \frac{1}{\Delta x} \int_{x-\frac{\Delta x}{2}}^{x+\frac{\Delta x}{2}} h(\xi) d\xi,$$

such that the spatial derivative in (2) is exactly approximated by a conservative finite difference formula at the cell boundaries,

$$\frac{du_i(t)}{dt} = \frac{1}{\Delta x}\left(h_{i+\frac{1}{2}} - h_{i-\frac{1}{2}}\right), \tag{3}$$

where $h_{i\pm\frac{1}{2}} = h(x \pm \frac{\Delta x}{2})$.

High order polynomial interpolations to $h_{i\pm\frac{1}{2}}$ are computed using known grid values of f. The classical fifth-order WENO scheme uses a 5-points stencil, hereafter named S^5, which is subdivided into three other 3-points stencils S_0, S_1, S_2, as shown in Fig. 1. The fifth-order polynomial approximation $\hat{v}_{i+\frac{1}{2}} = h_{i+\frac{1}{2}} + O(\Delta x^5)$ is built through the convex combination of interpolated values $\hat{f}_k\left(x_{i+\frac{1}{2}}\right)$, at $x_{i+\frac{1}{2}}$, by the third-degree polynomials $\hat{f}_k$, defined in each one of the stencils S_k:

$$\hat{v}_{i+\frac{1}{2}} = \sum_{k=0}^{2} \omega_k \hat{f}_k\left(x_{i+\frac{1}{2}}\right), \tag{4}$$

where

$$\hat{f}_k\left(x_{i+\frac{1}{2}}\right) = \sum_{j=0}^{2} c_{kj} f_{i-k+j} = h\left(x_{i+\frac{1}{2}}\right) + O(\Delta x^3). \tag{5}$$

The c_{kj} are Lagrangian interpolation coefficients (see [2]), which depend on the left-shift parameter $k = 0, 1, 2$, but not on the values f_i. The weights ω_k are defined as

$$\omega_k = \frac{\alpha_k}{\sum_{l=0}^{2} \alpha_l}, \qquad \alpha_k = \frac{d_k}{(\beta_k + \epsilon)^p}. \tag{6}$$

We refer to α_k as the unnormalized weights. The parameter ϵ is used to avoid the division by zero in the denominator and $p = 2$ is chosen to increase the difference of scales of distinct weights at non-smooth parts of the solution.

The smoothness indicators β_k measure the regularity of the k_th polynomial approximation $\hat{f}_k(x)$ at the Stencil S_k and are given by

$$\beta_k = \sum_{l=1}^{2} \Delta x^{2l-1} \int_{x_{i-\frac{1}{2}}}^{x_{i+\frac{1}{2}}} \left(\frac{d^l}{dx^l} \hat{f}_k(x) \right)^2 dx. \tag{7}$$

The expression of the β_k in terms of the cell values of f are given by

$$\beta_0 = \frac{13}{12} \left(f_{i-2} - 2f_{i-1} + f_i \right)^2 + \frac{1}{4} \left(f_{i-2} - 4f_{i-1} + 3f_i \right)^2, \tag{8}$$

$$\beta_1 = \frac{13}{12} \left(f_{i-1} - 2f_i + f_{i+1} \right)^2 + \frac{1}{4} \left(f_{i-1} - f_{i+1} \right)^2, \tag{9}$$

$$\beta_2 = \frac{13}{12} \left(f_i - 2f_{i+1} + f_{i+2} \right)^2 + \frac{1}{4} \left(3f_i - 4f_{i+1} + f_{i+2} \right)^2. \tag{10}$$

The coefficients $d_0 = \frac{3}{10}, d_1 = \frac{3}{5}, d_2 = \frac{1}{10}$ in (6) are called the ideal weights for the convex combination (4) since they generate the central upstream fifth-order scheme for the 5-points stencil S^5. The general idea of the weights definition (6) is that on smooth parts of the solution the smoothness indicators β_k are all small and about the same size, generating weigths ω_k that are good approximations to the ideal weights d_k. On the other hand, if the stencil S_k contains a discontinuity, β_k is $O(1)$ and the corresponding weight ω_k is small relatively to the other weights. This implies that the influence of the polynomial approximation of $h_{i\pm\frac{1}{2}}$ taken across the discontinuity is diminished up to the point where the convex combination (4) is essentially non-oscillatory. Figure 1 shows the case where stencil S_2 is discontinuous, yielding β_0 and β_1 to be much smaller than β_2. By (6), this results on ω_2 being a small number in the convex combination (4) (See also Fig. 3(a) of Section 3).

The process described above is called the WENO reconstruction step, for it reconstructs the values of $h(x)$ at the cell boundaries of the interval $I_i = [x_{i-\frac{1}{2}}, x_{i+\frac{1}{2}}]$ from its cell averaged values $f(x)$ in the intervals $S_k, k = 0, 1, 2$. In [3], truncation error analysis of the finite difference equation (3) led to sufficient conditions on the weights ω_k for the WENO scheme to achieve the formal fifth-order of convergence at smooth parts of the solution. It was found that at critical points, points where the first derivative of the solution vanishes, convergence degraded to only third order, a fact that was being hidden by the uniformization of the weights caused by the use of a large value for ϵ in (6). Since this analysis is relevant to the description of the new WENO scheme introduced at next section, we recall below its most important steps.

Substituting the convex combination (4) into the finite difference formula (3) we obtain:

$$\begin{aligned}
\hat{v}_{i+\frac{1}{2}} - \hat{v}_{i-\frac{1}{2}} &= \sum_{k=0}^{2} \omega_k^+ \hat{v}_{i+\frac{1}{2}} - \sum_{k=0}^{2} \omega_k^- \hat{v}_{i-\frac{1}{2}} \\
&= \left(\sum_{k=0}^{2} d_k \hat{v}_{i+\frac{1}{2}} - \sum_{k=0}^{2} d_k \hat{v}_{i-\frac{1}{2}} \right) + \sum_{k=0}^{2} (\omega_k^+ - d_k) \hat{v}_{i+\frac{1}{2}} - \sum_{k=0}^{2} (\omega_k^- - d_k) \hat{v}_{i-\frac{1}{2}} \\
&= \left(\hat{v}^c_{i+\frac{1}{2}} - \hat{v}^c_{i-\frac{1}{2}} \right) + \sum_{k=0}^{2} (\omega_k^+ - d_k) \left[h_{i+\frac{1}{2}} + A_k \Delta x^3 \right] - \sum_{k=0}^{2} (\omega_k^- - d_k) \left[h_{i-\frac{1}{2}} + B_k \Delta x^3 \right] \\
&= v'(x_i) \Delta x + O(\Delta x^6) + \sum_{k=0}^{2} (\omega_k^+ - d_k) A_k \Delta x^3 - \sum_{k=0}^{2} (\omega_k^- - d_k) B_k \Delta x^3.
\end{aligned}$$

Hence, the trunction error becomes

$$\frac{1}{\Delta x} \left(\hat{v}_{i+\frac{1}{2}} - \hat{v}_{i-\frac{1}{2}} \right) = v'(x_i) + O(\Delta x^5) + \sum_{k=0}^{2} (\omega_k^+ - d_k) A_k \Delta x^2 - \sum_{k=0}^{2} (\omega_k^- - d_k) B_k \Delta x^2, \tag{11}$$

where $\hat{v}^c_{i\pm\frac{1}{2}}$ are the fifth-order central upstream approximations to $h_{i\pm\frac{1}{2}}$ and ω_k^+ and ω_k^- are the WENO weights at $x_{i+\frac{1}{2}}$ and $x_{i-\frac{1}{2}}$, respectively, A_k and B_k are constants independent of Δx. It should be pointed out that due to normalization $\sum_{k=0}^{2} \omega_k^{\pm} = \sum_{k=0}^{2} d_k$ and that $\mathrm{O}(\Delta x^5)$ is still obtained after the division by Δx in the difference of the central approximations $\hat{v}^c_{i\pm\frac{1}{2}}$, because of cancellation of identical $\mathrm{O}(\Delta x^5)$ terms. Thus, a sufficient condition on the weights (6) to get a fifth-order truncation error at (3) is given by

$$\omega_k^{\pm} \quad = \quad d_k + O(\Delta x^3), \quad k = 0, 1, 2. \tag{12}$$

Considering, for simplicity, that $\epsilon = 0$, it is easily seen from (6) that if the smoothness indicators satisfy $\beta_k = D(1 + O(\Delta x^3))$, for a constant D independent of k, then the unnormalized weights also satisfy $\alpha_k = D(1 + O(\Delta x^3))$ and $\omega_k = d_k + O(\Delta x^3)$ (see [3]).

It is easily seen that for the classical scheme, and a sufficiently smooth solution,

$$\beta_k = D(1 + O(\Delta x^2)) \text{ and } \omega_k = d_k + O(\Delta x^2), \tag{13}$$

which does not satisfy (12), yielding convergence order less than 5. In [3], the weights ω_k were modified by a mapping function that increased the approximation to the ideal weights d_k to the required third order $O(\Delta x^3)$. The mapping function $g_k(\omega)$ was defined as

$$g_k(\omega) = \frac{\omega\left(d_k + d_k^2 - 3d_k\omega + \omega^2\right)}{d_k^2 + \omega\left(1 - 2d_k\right)}. \tag{14}$$

It is a nondecreasing monotone function with the following properties:

- $0 \le g_k(\omega) \le 1, \quad g_k(0) = 0$ and $g_k(1) = 1$.
- $g_k(\omega) \approx 0$ if $\omega \approx 0$; $\quad g_k(\omega) \approx 1$ if $\omega \approx 1$.
- $g_k(d_k) = d_k$, $g_k'(d_k) = g_k''(d_k) = 0$.
- $g_k(\omega) = d_k + O(\Delta x^{3r})$, if $\omega = d_k + O(\Delta x^r)$.

At critical points of the solution, the order of the classical scheme decreases more since we only obtain $\beta_k = D(1 + O(\Delta x))$, if $f'' \neq 0$, and $\beta_k = D(1 + O(1))$, if $f'' = 0$ (see Equations (15)-(17) below). Thus, the mapping does improve the order of the classical scheme at the critical points of first order, but it cannot help when too many derivatives vanish.

For problems with shocks, the $O(1)$ truncation error at the discontinuities diminishes the advantages of such order improvements. Nevertheless, the results obtained by the mapped scheme are clearly superior to the classical scheme results. Distinctly from [3], we do not credit the enhancements of the numerical solution to the higher order of the mapped scheme at critical points, but to the smaller dissipation that it provides when assigning larger weights to discontinuous stencils, as we shall see in the next section. We will also see that the new smoothness indicators proposed in this work yield even larger weights than the mapped WENO to stencils with discontinuities, generating even better solutions.

3 An Improved WENO Scheme

In this section we devise a new set of weights that satisfies the sufficient condition (12) and recovers the formal order of accuracy at the smooth regions of the solution. The novel idea is the use of higher order smoothness indicators at the formula for the weights of the convex combination (4). In order to define the new smoothness indicators of higher order, we need the following Taylor series expansions for the smoothness indicators β_k of (7):

$$\beta_0 = v'^2\Delta x^2 + \left(\frac{13}{12}v''^2 - \frac{2}{3}v'v'''\right)\Delta x^4 - \left(\frac{13}{6}v''v''' - \frac{1}{2}v'v''''\right)\Delta x^5 + O(\Delta x^6), \quad (15)$$

$$\beta_1 = v'^2\Delta x^2 + \left(\frac{13}{12}v''^2 + \frac{1}{3}v'v'''\right)\Delta x^4 + O(\Delta x^6), \quad (16)$$

$$\beta_2 = v'^2\Delta x^2 + \left(\frac{13}{12}v''^2 - \frac{2}{3}v'v'''\right)\Delta x^4 + \left(\frac{13}{6}v''v''' - \frac{1}{2}v'v''''\right)\Delta x^5 + O(\Delta x^6). \quad (17)$$

The higher order new smoothness indicator τ_5 is defined as the difference between β_0 and β_2, namely

$$\tau_5 = \max\left(|\beta_0 - \beta_2|, \epsilon\right), \quad (18)$$

where ϵ is a small number used to ensure that $\tau_5 \neq 0$. We see from (10) and from equations (15)-(17) that τ_5 is a measure of the higher derivatives of the function, when they exist, and is computed using the whole 5-points stencil S^5. The following properties of τ_5 are important for the definition of the new WENO scheme:

- If S^5 contains neither discontinuities, nor critical points, then $\tau_5 = O(\Delta x^5) \ll \beta_k$, for $k = 0, 1, 2$;
- if the solution is continuous at some of the S_k, but discontinuous in the whole S^5, then $\beta_k \ll \tau_5$, for those k where the solution is continuous;
- $\tau_5 \leq \max_k \beta_k$.

Figure 2 shows the values of β_k and τ_5 for the discontinuous function:

$$u(x,0) = f(x) = \begin{cases} -\sin(\pi x) - \frac{1}{2}x^3 & -1 < x < 0 \\ -\sin(\pi x) - \frac{1}{2}x^3 + 1 & 0 \leq x \leq 1 \end{cases}. \quad (19)$$

consisting of a piecewise sine function with a jump discontinuity at $x = 0$. Note that τ_5 is only comparable to one of the β_k at stencils that include the discontinuity.

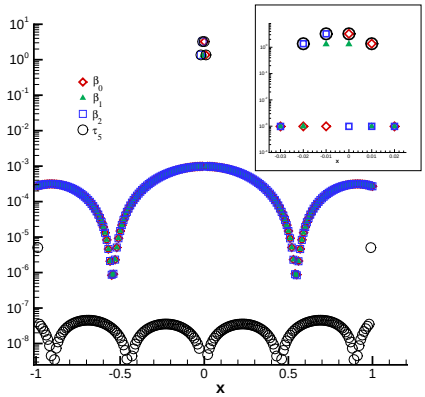

Figure 2: Values of β_k and τ_5 for the discontinuous periodic function (19).

The following notation will be used in order to distinguish between the 3 different WENO schemes considered in this work. The mapped weights of [3] are denoted as ω_k^M and the resulting mapped WENO scheme as WENO-M. The new WENO scheme, introduced below, is referred as WENO-Z and the superscript z is added to all quantities related to it. To keep a coherent notation throughout the article, the classical weights and smoothness indicators carry no superscript, although, the classical WENO scheme of [2] is referred as WENO-JS.

The new smoothness indicators β_k^z are defined as

$$\beta_k^z = \frac{\beta_k + \epsilon}{\beta_k + \tau_5}, \tag{20}$$

and the new weights ω_k^z as

$$\omega_k^z = \frac{\alpha_k^z}{\sum_{l=0}^{2} \alpha_l^z}, \quad \alpha_k^z = \frac{d_k}{\beta_k^z}, \quad k = 0, 1, 2. \tag{21}$$

Rigorously speaking, β_k^z are not smoothness indicators, for they are all close to 1 at smooth parts of the solution. They are in fact the normalization of the classical smoothness indicators by higher order information contained in the larger stencil S^5.

Remark 1 *Note that $p = 1$ in the definition of the unnormalized weights α_k^z. Numerical experiments showed that the use of $p = 2$, as in the definition of the classical unnormalized weights α_k, led to an unstable scheme, for it amplified too much the ratio (24). This is the opposite way that was taken in the definition of the classical weights where $p = 2$ was used to increase the distance between a continuous and a discontinuous stencil and, therefore, decrease the importance of this last one at the final convex combination.*

Remark 2 *The role of ϵ was discussed in [3], where it was shown that the large value of 10^{-6}, commonly suggested in the literature, would dominate over the smoothness indicators β_k at the denominators of the definition of the classical weights. Due to (13), a smaller value for ϵ degrades the order of the classical scheme, particularly at critical points. In this work, we use much smaller values of ϵ for all schemes, in order to make apparent their real truncation errors. In other words, the parameter it is reduced to play only its original role of not allowing vanishing denominators at the weights definitions.*

In the following, we show that $\omega_k^z = d_k + O(\Delta x^3)$ at smooth parts of the solution and that bigger weights are assigned to discontinuous stencils with the new scheme WENO-Z. We take $\epsilon = 0$ at the analyses below due to the reasons given in Remark 2.

We now compute the order of approximation of the weights in (21) to the ideal weights d_k. For the sake of clarity, we will not consider the case of critical points initially. Thus, at smooth regions of the solution, not containing critical points, we see from Equations (15)-(17) that $\beta_k \approx O(\Delta x^2)$, yielding

$$\beta_k^z = \left(1 + \tau_5 \beta_k^{-1}\right)^{-1} = 1 + O\left(\Delta x^3\right), \quad k = 0, 1, 2. \tag{22}$$

It follows that

$$\omega_k^z = \frac{d_k \left(1 + \tau_5 \beta_k^{-1}\right)}{\sum_{j=0}^{2} d_j \left(1 + \tau_5 \beta_l^{-1}\right)} = \frac{d_k \left(1 + O(\Delta x^3)\right)}{\sum_{j=0}^{2} d_l \left(1 + O(\Delta x^3)\right)} = d_k + O(\Delta x^3), \quad k = 0, 1, 2. \tag{23}$$

Thus, the new weights ω_k^z satisfy the sufficient condition (12), providing the formal fifth order of accuracy to the WENO-Z scheme at the smooth regions of the solution.

Next, we examine the behavior of ω_k^z on stencils containing discontinuities with respect to the classical weights. The analysis can be performed by looking at the behavior of the smoothness indicators β_k^z. Consider the simple case of a shock localized in stencil S_2, while the solution in stencils S_0 and S_1 are smooth (see Fig. 1), the ratios between the smaller smoothness indicators $\beta_k, k = 0, 1$ and the largest one, β_2, are increased with for the new smoothness indicators β_k^z:

$$\frac{\beta_k^z}{\beta_2^z} = \frac{\beta_k}{\beta_2} \frac{\beta_2 + \tau_5}{\beta_k + \tau_5} \geq \frac{\beta_k}{\beta_2}, \quad k = 0, 1, \tag{24}$$

using the fact that $\beta_2 > \beta_k, k = 0, 1$.

Similarly, the relative importance of the stencil S_2 containing the discontinuity in the new convex combination is also increased, since:

$$\frac{\omega_2^z}{\omega_k^z} = \frac{d_2}{d_k}\frac{\beta_k^z}{\beta_2^z} \geq \frac{\omega_2}{\omega_k}, \quad k = 0, 1, \tag{25}$$

Let us now compare the sizes of the weights ω_k for the classical WENO-JS, WENO-M and the new WENO-Z schemes at the first step of the numerical solution of the wave equation $u_t = u_x$, with periodic initial condition given by (19).

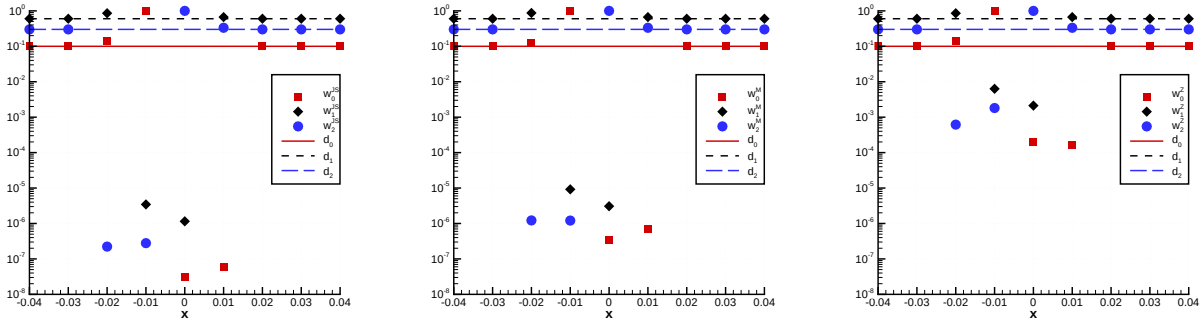

(a) WENO-JS (b) WENO-M (c) WENO-Z

Figure 3: The distribution of the ideal weights d_k and the weights $\omega_k, k = 0, 1, 2$ for (a) WENO-JS, (b) WENO-M and (c) WENO-Z schemes at the first step of the numerical solution of the wave equation $u_t = u_x$, with periodic initial condition given by (19). The ideal weights $d_k, k = 0, 1, 2$ are shown with line styles and the weights $\omega_k, k = 0, 1, 2$ are shown with symbols. The vertical axes are shown in $\log_{10}$ scale.

Figures 3(a)-(c) show the weights ω_k, for the WENO-JS, WENO-M and WENO-Z schemes plotted together with the ideal weights d_k,where the vertical axis is in $\log_{10}$ scale. Away from the discontinuity, at $x = 0$, the weights ω_k (symbols) for all schemes correctly match the corresponding ideal weights d_k (lines). The first location where the five-points stencil S^5 encounter the discontinuity is at $x = -0.01$. At this grid point, the rightmost stencil S_2 has its weight ω_2 decreased to a much smaller value than ω_0 and ω_1, while these two are slightly increased to reflect their larger relevance at the reconstruction step. At $x = -0.005$, the discontinuity is present at S_1 and S_2 and a small value is also assigned to ω_1, yielding $\omega_0 \approx O(1)$. A symnmetric scenario occurs at $x = 0.005$, where ω_2 assumes the largest value. While this situation is general for all schemes, the main difference is at the ratios between the weights for discontinuous and continuous stencils, as discussed above. While WENO-JS sets very small values for the discontinuous stencils, around 10^{-8}, and the mapping of WENO-M generates a small increase on these values, WENO-Z yields a more substantial increase to 10^{-4}.

Figure 4 shows the numerical solutions of the wave equation $u_t = u_x$ at $t = 8$, for all three schemes, along with the exact solution. Note that the numerical solution generated by WENO-Z is qualitatively similar to the one generated by WENO-M, being slightly sharper at the discontinuity. It can also be observed that both schemes show distinctly better results than the classical WENO-JS.

4 Numerical Experiments

In this section we compare the numerical performance of the new weno scheme, WENO-Z, with the classical WENO-JS and its improved version WENO-M. We show at first that WENO-Z is indeed a fifth-order scheme by showing its errors with a smooth scalar advection problem. We also compare its behavior in

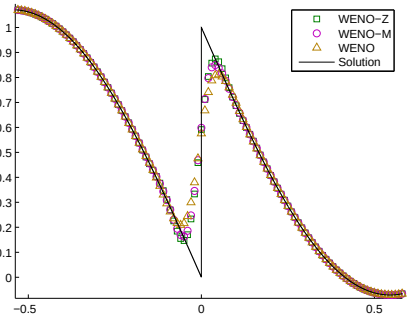

Figure 4: Numerical solutions of the linear wave equation with the discontinuous initial condition (19) at $t = 8$ for all three schemes. The exact solution is shown with a solid line.

the advection of discontinuous functions with the other two schemes. Finally, the one dimensional Euler equations are solved for the Mach 3 shock density wave interaction and the interactive blastwaves problems.

4.1 Linear advection problems

In this section, the new scheme, WENO-Z, is used to solve the linear transport equation with smooth and discontinuous initials conditions. Table I shows the L_1, L_2 and L_∞ errors, along with the respective orders of convergence, when WENO-Z is applied to the numerical solution of the linear advection of the scalar smooth function:

$$u(x, 0) = \sin(2\pi x).$$

One can see that WENO-Z, with the new weights ω_k^z, achieves fifth-order convergence for smooth problems.

N	L_1 Error	Order	L_2 Error	Order	L_∞ Error	Order
25	7.9e-1		6.2e-1		6.5e-1	
50	3.5e-2	4.50	2.8e-2	4.49	2.8e-2	4.55
100	1.1e-3	4.98	8.8e-4	4.98	8.8e-4	4.98
200	3.5e-5	5.00	2.7e-5	5.00	2.7e-5	5.00
400	1.1e-6	5.00	8.6e-7	5.00	8.6e-7	5.00

Table I: The L_1, L_2 and L_∞ errors of the linear wave equation, with a smooth initial condition, as computed by the WENO-Z scheme with the new weights ω_k^z.

Next, WENO-Z is tested with the linear transport of discontinuous functions, in the case of an initial condition consisting of a Gaussian, a triangle, a square-wave and a semi-ellipse, given by

$$u(x,0) = \begin{cases} \frac{1}{6}\left[G(x,\beta,z-\delta) + 4G(x,\beta,z) + G(x,\beta,z+\delta)\right] & ,x \in [-0.8,-0.6] \\ 1 & ,x \in [-0.4,-0.2] \\ 1 - |10(x-0.1)| & ,x \in [0,0.2] \\ \frac{1}{6}\left[F(x,\alpha,a-\delta) + 4F(x,\alpha,a) + F(x,\alpha,a+\delta)\right] & ,x \in [0.4,0.6] \\ 0 & ,\text{otherwise} \end{cases}, \quad (26)$$

$$G(x,\beta,z) = e^{-\beta(x-z)^2}, \quad (27)$$

$$F(x,\alpha,a) = \sqrt{\max\left(1-\alpha^2(x-a)^2, 0\right)}, \quad (28)$$

(a) Solution (b) Error

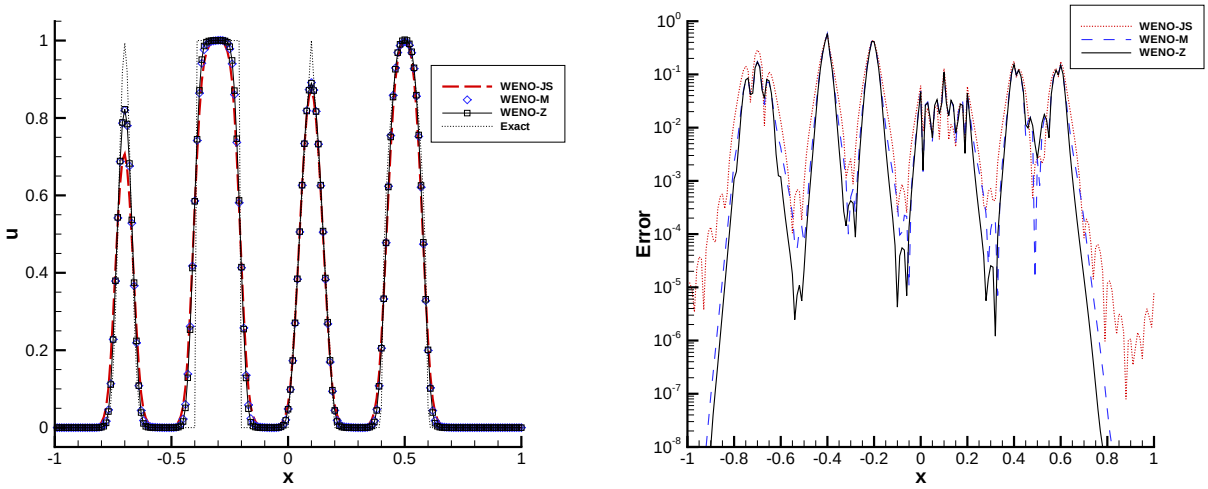

Figure 5: Numerical solution and absolute pointwise error of the advection equation with the discontinuous initial condition (28) as computed by WENO-JS, WENO-M and WENO-Z with $N = 200$ at $t = 8$.

(a) Solution (b) Error

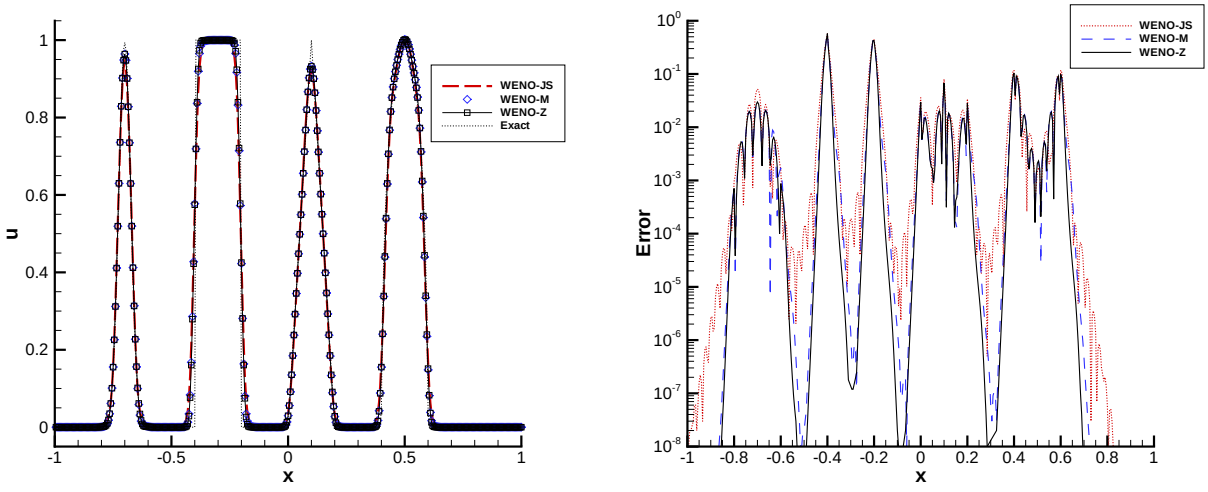

Figure 6: Numerical solution and absolute pointwise error of the advection equation with the discontinuous initial condition (28) as computed by WENO-JS, WENO-M and WENO-Z with $N = 400$ at $t = 8$.

where the constants are $z = -0.7, \delta = 0.005, \beta = \frac{\log 2}{36\delta^2}, a = 0.5$ and $\alpha = 10$.

Figures 5 and 6 show that WENO-Z behaves quantitatively and qualitatively equivalent to WENO-M with regards to the improvements over WENO-JS, but WENO-Z still shows the best results of all three schemes. Also, as indicated in the figures, the smaller dissipation of WENO-Z generates slightly better results on the various corners and pikes of the solution. Note also that the theoretical deficiency of WENO-Z at the critical points does not seem to influence the performance at the capturing of the several discontinuities of the solution. This is expected since the mapping of WENO-M increases the order from 3 to 5 at the critical points for smooth solutions only, while at the discontinuities, the overall global rate of convergence of the WENO schemes is only first order.

4.2 The Euler equations

In this section we present numerical experiments with the system of Euler Equations for gas dynamics in strong conservation form:

$$\mathbf{Q}_t + \mathbf{F}_x = 0, \tag{29}$$

where

$$\mathbf{Q} = (\rho, \rho u, E)^T, \quad \mathbf{F} = (\rho u, \rho u^2 + P, (E + P)u)^T, \tag{30}$$

and the equation of state is given by

$$P = (\gamma - 1)\left(E + \frac{1}{2}\rho u^2\right), \qquad \gamma = 1.4. \tag{31}$$

The ρ, u, P, E are the density, velocity, pressure and total energy respectively. Following [1], the hyperbolicity of the Euler equations admits a complete set of right and left eigenvectors for the Jacobian of the system. The eigenvalues and eigenvectors are obtained via the linearized Riemann solver of Roe [4] and the first order Lax-Friedrichs flux is used as the low order building block for the high order reconstruction step of WENO (see equation (2.5) in [1]). After projecting the fluxes on the characteristic fields via the left eigenvectors, the high order WENO reconstruction step is applied to obtain the high order approximation at the cell boundaries, which are projected back into physical space via the right eigenvectors. The resulting system of ODEs is advanced in time using the third order Total Variation Diminishing Runge-Kutta scheme (RK-TVD). See [1] for further details of the algorithm.

4.2.1 Shock-density wave interaction

Consider the one dimensional Mach 3 shock-entropy wave interaction [5], specified by the following initial conditions:

$$(\rho, u, P) = \begin{cases} (\quad 3.857143, \quad 2.629369, \quad 10.33333 \quad) & -5 \le x < -4 \\ (\quad 1 + 0.2\sin(kx), \quad 0, \quad 1 \quad) & -4 \le x \le 5 \end{cases}, \tag{32}$$

where $x \in [-5, 5]$ and $k = 5$. The solution of this problem consists of a number of shocklets and fine scales structures which are located behind a right-going main shock.

Figure 7(a)-(b) provides a comparison for all schemes at $t = 1.8$ with an increasing number of points. We shall refer to the solution computed by the WENO-M scheme with $N = 2000$ points as the "exact" solution. At a low resolution, $N = 200$, as shown in Fig. 7(a), WENO-M and WENO-Z capture much more features of the solution than WENO-JS, particularly at the high frequency waves behind the shock, with WENO-Z achieving deeper valleys and higher pikes than WENO-M. Increasing the resolution to $N = 300$, as shown in Fig. 7(b), we see that convergence of WENO-M and WENO-Z is faster than WENO-JS.

At Fig. 8, the wave number k is increased to 10, yielding rougher numerical approximations at the sine wave density field perturbation. The same observation can be made similar to one made in the previous $k = 5$ case, where the improvement of the more accurate schemes WENO-M and WENO-Z over the classical WENO-JS is more distinct.

(a) $N = 200$ (b) $N = 300$

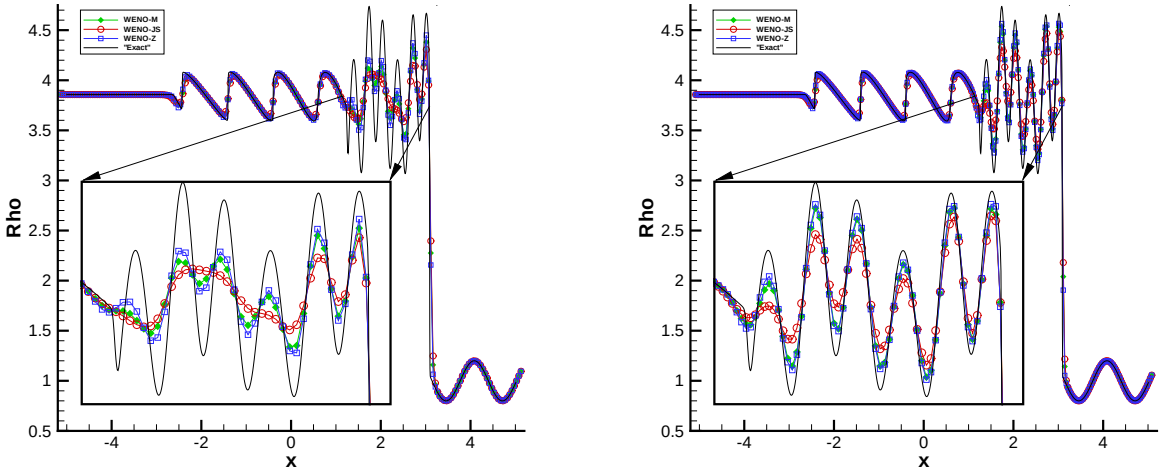

Figure 7: Solution of the Mach 3 shock density wave interaction with $k = 5$ as computed by WENO-JS, WENO-M and WENO-Z schemes with (a) $N = 200$, (b) $N = 300$ points. The "exact" solution is computed by the WENO-M scheme with $N = 2000$ points.

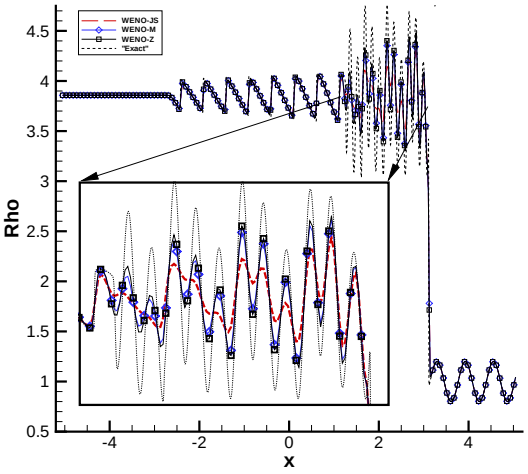

Figure 8: Solution of the Mach 3 shock density wave interaction with $k = 10$ computed by WENO-JS, WENO-M and WENO-Z with $N = 510$ points. For clarity, only symbols at every fourth data point are plotted. The "exact" solution is computed by the WENO-M scheme with $N = 2000$ points.

4.2.2 Interacting Blastwaves

The one dimensional Blast waves interaction problem by Woodward and Collela [7] has the following initial configuration, with reflective boundary conditions:

$$(\rho, U, P) = \begin{cases} (\ 1, \ 0, \ 1000\ ) & 0 \le x < 0.1 \\ (\ 1, \ 0, \ 0.01\ ) & 0.1 \le x < 0.9 \\ (\ 1, \ 0, \ 100\ ) & 0.9 \le x \le 1.0 \end{cases} . \tag{33}$$

The initial pressure gradients generate two density shock waves that collide and interact later in time, forming a profile as shown in Fig. 9 at $t = 0.038$. All three schemes converge, as the number of points increase, to the reference solution computed by the WENO-M with $N = 4000$ points. As before, WENO-M and WENO-Z show an improved convergence with respect to WENO-JS, due to their smaller dissipation. Figure 10 presents a separate, and more detailed, comparison between WENO-M and WENO-Z, at two different portions of the domain and different numbers of points. Careful examination of Fig. 10(a) shows that WENO-Z obtains a sharper resolution of the shock near $x = 0.65$ and a higher pike near $x = 0.78$. In Fig. 10(b), the high gradient structure at $x = 0.86$ is clearly better resolved with WENO-Z, as well as the contact discontinuity near $x = 0.8$, with $N = 800$ points.

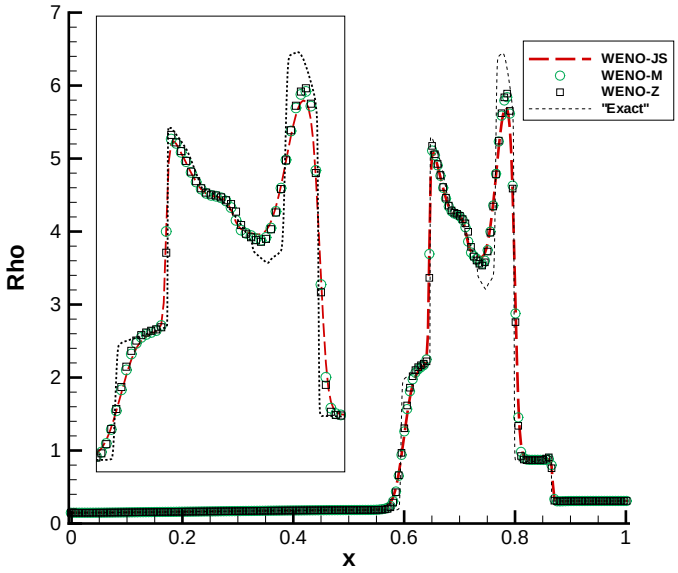

Figure 9: Solution of the interactive blastwaves problem computed by WENO-JS, WENO-M and WENO-Z with $N = 400$ points. For clarity, only symbols at every other data point are plotted. The "exact" solution is computed by the WENO-M scheme with $N = 4000$ points.

5 Conclusions

We have devised an improved version of the fifth order WENO scheme that makes use of higher order information on the regularity of the solution already contained in the original framework of the classical WENO scheme. A set of new smoothness indicators was devised, resulting in a less dissipative approximation

(a) $x \in [0.625, 0.800]$ (b) $x \in [0.790, 0.875]$

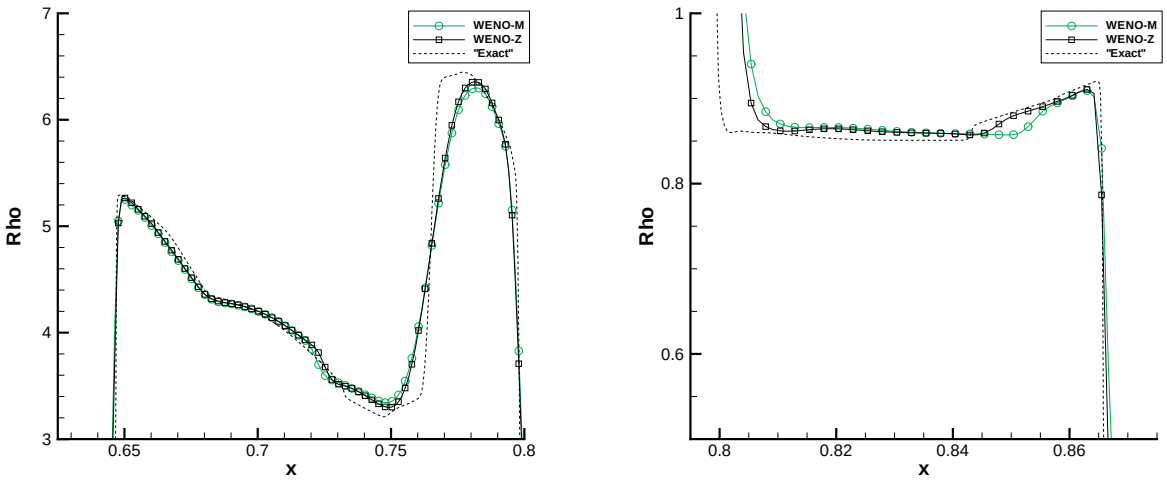

Figure 10: Zoom in regions of the solution of the interactive blastwaves problem computed by WENO-M and WENO-Z with $N = 800$ points. For clarity, only symbols at every other data point are plotted. The "exact" solution is computed by the WENO-M scheme with $N = 4000$ points.

near discontinuities. To demonstrate this, we have compared the new WENO scheme with the classical WENO scheme of Jiang and Shu and the mapped WENO scheme of Hendrick et al. in the one dimensional solution of the Euler equations, in particular, the Mach 3 shock density wave interaction and the interactive blastwaves problems. These results showed that the new WENO scheme substantially improves on the classical WENO scheme, generating numerical solutions that are slightly better than the mapped WENO. The WENO scheme proposed in this article is a simple and natural improvement on the classical smoothness indicators with no additional computational cost. Nevertheless, it inherits the same theoretical deficiency of the classical WENO at critical points, no relevant influence at problems with shocks have been found. Research is currently underway to extend the idea to higher order WENO reconstruction schemes and will be reported on an upcoming paper.

6 Acknowledgements

The first and second authors have been supported by CNPq, grant 300315/98-8. The third author gratefully acknowledges the support of this work by the DOE under contract number DE-FG02-98ER25346 and AFOSR under contract number FA9550-05-1-0123, and would also like to thanks the Departamento de Matemática Aplicada, IM-UFRJ, for hosting his visit.

References

[1] D. Balsara and C. W. Shu, *Monotonicity preserving weighted essentially non-oscillatory schemes with increasingly high order of accuracy*, J. Comp. Phys. **160**, pp. 405–452 (2000)

[2] G. S. Jiang and C. W. Shu, *Efficient Implementation of Weighted ENO Schemes*, J. Comp. Phys. **126**, pp. 202–228 (1996)

[3] A. K. Henrick, T. D. Aslam and J. M. Powers, *Mapped weighted essentially non-oscillatory schemes: Achieving optimal order near critical points*, J. Comp. Phys. **207**, pp. 542–567 (2005)

[4] P. L. Roe, *Approximation Riemann solvers, parameter vectors, and difference schemes*, J. Comput. Phys. **43**, pp. 357 (1981)

[5] C. W. Shu and S. Osher, *Efficient Implementation of Essentially Non-oscillatory Shock-Capturing Schemes*, J. Comp. Phys. **77**, pp. 439–471 (1988)

[6] C. W. Shu and S. Osher, *Efficient Implementation of Essentially Non-oscillatory Shock-Capturing Schemes, II*, J. Comp. Phys. **83**, No. 1, pp. 32–78 (1989)

[7] P. Woodward and P. Collela, *The numerical simulation of two dimensional fluid flow with strong shocks*, J. Comp. Phys. **54**, pp. 115–173 (1984)